NANOSYSTEMS:
PHYSICS, CHEMISTRY, MATHEMATICS

Enyashin A.N. *Nanosystems: Phys. Chem. Math.*, 2025, **16** (5), 693–699.
http://nanojournal.ifmo.ru
DOI 10.17586/2220-8054-2025-16-5-693-699

Original article

GdI_3 fullerenes: a DFT study of structural and electronic properties

Andrey N. Enyashin

Institute of Solid State Chemistry UB RAS, Ekaterinburg, Russia

enyashin@ihim.uran.ru

PACS 61.48.-c, 73.90.+f

ABSTRACT The existence of zero-dimensional fullerene-like gadolinium(III) iodide is proposed. The models of tetrahedral, octahedral and icosahedral GdI_3 fullerenes with the size up to ∼1000 atoms are constructed. Their stability and electronic properties are investigated by means of a density functional theory method. Similarly to other known inorganic fullerenes and nanotubes, the strain energies of GdI_3 fullerenes decrease with the radii increase, exceeding always the strain energies of GdI_3 nanotubes of the same radii. At that octahedral and icosahedral morphologies are the most preferable. Irrespective size and morphology, all considered GdI_3 fullerenes are semiconductors with possibly ferromagnetic ordering at extremely low temperatures. The HOMO-LUMO gaps of GdI_3 fullerenes are narrower on 1.1 – 1.7 eV, when comparing to the band gap of the flat GdI_3 monolayer.

KEYWORDS gadolinium triiodide, fullerenes, DFT calculations

ACKNOWLEDGEMENTS This study was carried out within the framework of the state assignment for the Institute of Solid State Chemistry UB RAS (No. 124020600024-5).

FOR CITATION Enyashin A.N. GdI_3 fullerenes: a DFT study of structural and electronic properties. *Nanosystems: Phys. Chem. Math.*, 2025, **16** (5), 693–699.

1. Introduction

Trivalent gadolinium (Gd^{3+}) is an ion that possesses the maximum number of unpaired electrons of any stable ions due to the presence of 7 unpaired electrons in the inner $4f$-electronic shell. Exhibiting large magnetic moments and achievable low magnetic ordering temperatures, both solid and molecular compounds of Gd^{3+} are attractive as magnetic refrigerants [1, 2]. Yet, Gd^{3+} ions are more honored in biomedical applications as working element of various contrast agents. At temperatures above 20 °C they hold innate paramagnetic properties and a high sensitivity to external magnetic field, allowing enhanced magnetic resonance imaging (MRI) [3]. Besides, the attenuation of X-rays by gadolinium can be greater than that of iodine, which opens a perspective to design the more sensitive radiographic contrast agents and even the agents with dual MRI and radiographic modality [4]. Association of gadolinium and iodine in a single compound like GdI_3 might enhance X-rays' attenuation, which can be further utilized for sensitization of composite luminescent materials for a particle radiation detection [5].

Apart of the design of new gadolinium chelates [6] or endofullerenes ("gadofullerenes") [7], a significant effort was undertaken to improve the MRI contrast performance by means of gadolinium accumulation using inorganic compounds. Chimie douce encapsulation of $GdCl_3$ into ultra-short and narrow carbon nanotubes [8, 9] produced both exo- and endohedral composites of highly-defective nanotubes with superparamagnetic clusters of Gd^{3+} ions and Gd atoms ("gadonanotubes"), amplifying MRI in order of magnitude [10]. High-temperature imbibition of GdI_3 into multi-walled carbon nanotubes [11] or into inorganic WS_2 nanotubes [12] yielded their endohedral composites with one-dimensional nanoribbons or nanotubes of GdI_3, which remain paramagnetic and could be considered as potential MRI contrast agents protected by carbon or WS_2 wall. Fabrication of one-dimensional GdI_3 and concomitant gadolinium compounds has prompted theoretical research of capillarity of carbon and non-carbon nanotubes in relation to molten GdI_3, $GdBr_3$ and $GdCl_3$ using molecular dynamics simulations [13] as well as stability and electronic properties of individual GdI_3 nanotubes using quantum-chemical calculations [14]. Yet, an in-depth research of both the properties and the metabolism of such nanocomposites is still required.

Morphology of Gd^{3+}-ion containing nanoparticles, especially, GdI_3 as a dual contrast agent for MRI and X-ray imaging may be a tool for manipulation on its magnetic, magnetocaloric, optic and X-ray absorption properties. So far, only one-dimensional nanostructures of GdI_3 were reported [11, 12, 14], while corresponding zero-dimensional nanostructures like fullerenes or fullerene-like particles have been not even predicted. This can be found in drastic contrast to layered halides of d- and p-elements – $NiCl_2$ [15], $NiBr_2$ [16], $CdCl_2$ [17], CdI_2 [18], LaF_3 [19], which can be folded up into both nanotubes and fullerenes or fullerene-like nanoparticles [20, 21]. Here, we suggest the construction principles and explore theoretically the stability and electronic properties of GdI_3 fullerenes as an essential prerequisite to understanding the chemistry and physics of gadolinium compounds with zero-dimensional morphology.

2. Computational details

The spin-polarized calculations of all nanostructures were performed within the framework of the density-functional theory (DFT) as implemented in the SIESTA 4.0 software [22, 23]. The exchange-correlation potential was described within the Generalized Gradient Approximation with the Perdew–Burke–Ernzerhof parameterization. The core electrons were treated within the frozen core approximation, applying norm-conserving Troullier–Martins pseudopotentials. The valence electron configurations were chosen as $6s^2 5d^1 4f^7$ for Gd and $5s^2 5p^5$ for I with the wave-functions described using the double-ζ polarized basis set. The real-space grid used for the numeric integrations was set to correspond to the energy cutoff of 300 Ry. All calculations were performed using the full geometry optimization until the maximum residual force component of 0.05 eV/Å.

3. Results and discussion

3.1. Construction principles of GdI_3 fullerenes

In the thermodynamically stable polymorph of gadolinium triiodide, Gd^{3+} cations are arranged in the honeycomb networks in edge-sharing octahedral coordination by six I^- anions, which are each bonded to two Gd^{3+} cations. The resulting three-atom thick layers of composition GdI_3 are hexagonal and form via vdW interaction rhombohedral crystal with the BiI_3 structure type (space group R-3) [24]. The unstable polymorph of GdI_3 is stabilized at pressures 1 – 4 GPa as orthohombic crystal with the $PuBr_3$ structure type (space group Cmcm), where Gd^{3+} cations adopt a bicapped trigonal prismatic coordination by eight I^- anions [25]. Our preliminary geometry optimizations of both the bulk and the monolayer of GdI_3 have revealed preservation of their hexagonal symmetries and have validated the chosen calculation scheme. The equilibrium lattice parameters of the bulk GdI_3 were found as $a = 7.39$ Å and $c = 19.69$ Å in a fair agreement with experimental data $a = 7.54$ Å and $c = 20.83$ Å [24]. Single GdI_3 layer undergoes a slight in-plane contraction, resulting in the equilibrium lattice parameter $a = 7.35$ Å.

While the bending of a layer in one dimension, such as into a seamless nanotube, does not impose any constraint on the structure of the layer, but mechanical stress, the construction of the fully closed shell as a layer bent in two dimensions imposes a number of topological restrictions. Construction principles of both carbon and inorganic fullerenes rely on insertion of point defects into monolayer, which can provide a surface with positive curvature and serve as vertices of polyhedral fullerenes. The most famous example is the closure of graphene into a fullerene, which requires introduction of such defects as 12 pentagons into its honeycomb lattice [26]. A stable closure of layers of binary compounds with triangular lattices like hexagonal BN, metal dichalcogenides or dihalides requires introduction of 6 tetragons ("square-like defects") to preserve alternant heteronuclear bonding [21]. Then, the facets of fullerenes are represented as triangular or rhombi-like layers' patches, where the sewing of equilateral facets may release the fullerenes with perfect symmetric morphology of icosahedron for graphene or octahedron for inorganic layers.

While GdI_3 is a binary compound, cationic sublattice of its layer is honeycomb like graphene. Therefore, the first trial to build the atomistic models of GdI_3 fullerenes could rely on the known generations of carbon fullerenes. However, simple transfer of construction principles is not applicable here: symmetry of GdI_3 layer (point group D_3) is lower, than symmetry of graphene (point group D_6), imposing an additional constrain on sewing of anionic sublattice of GdI_3 facets at edges. The most obvious construction of the edge between two GdI_3 facets consists of the boundary of Gd^{3+} cations with trigonal prismatic coordination by I^- anions (Fig. 1). Such type of boundary violates neither the coordination numbers of ions nor the stoichiometry of compound. Prismatic coordination of cations is typical for layered compounds with a high degree of covalent bonding like chalcogenides and pnictogenides [27]. Yet, the layered oxides and nitrides with a more ionic bonding and, simultaneously, with prismatic coordination of cations are known, too [28]. The proposed prismatic coordination of Gd^{3+} cations is also reminiscent of the bicapped prismatic coordination in the high-pressure GdI_3 polymorph [25]. Moreover, the Gd–I phase diagram possesses gadolinium diiodide GdI_2 with the only prismatic coordination of Gd^{2+} cations [29].

These simple construction principles allowed design of three families of stoichiometric GdI_3 fullerenes with different right morphologies (Fig. 1). First family included icosahedral GdI_3 fullerenes with cationic sublattice equivalent to the lattice of carbon fullerenes from C_{60} family and consisting of $N = 60n^2$ units, where n is an integer. Second and third families were represented by octahedral and tetrahedral GdI_3 fullerenes consisting of $N = 24n^2$ and $N = 12n^2$ units, respectively. Cationic sublattices of the latter families are not related to the lattices of classic carbon fullerenes, since containing either 4 trigons or 6 tetragons as vertices. Though, irrespective the fullerene morphology the facets and the edges consist, respectively, of octahedral and prismatic GdI_6 coordination polyhedra.

The physical meaning of n is the half-quantity of Gd^{3+} cations forming a single edge. In the following, stability and electronic properties of GdI_3 nanoicosahedra with n = 1, 2, GdI_3 nanooctahedra and GdI_3 nanotetrahedra with n = 1 – 3 are discussed.

3.2. Thermodynamic stability of GdI_3 fullerenes

Fundamental criterion for thermodynamic stability of a hollow nanostructure (fullerene, nanotube, nanoroll etc.) is the energy of nanostructure relative to corresponding infinite planar layer, so-called strain energy. An early study

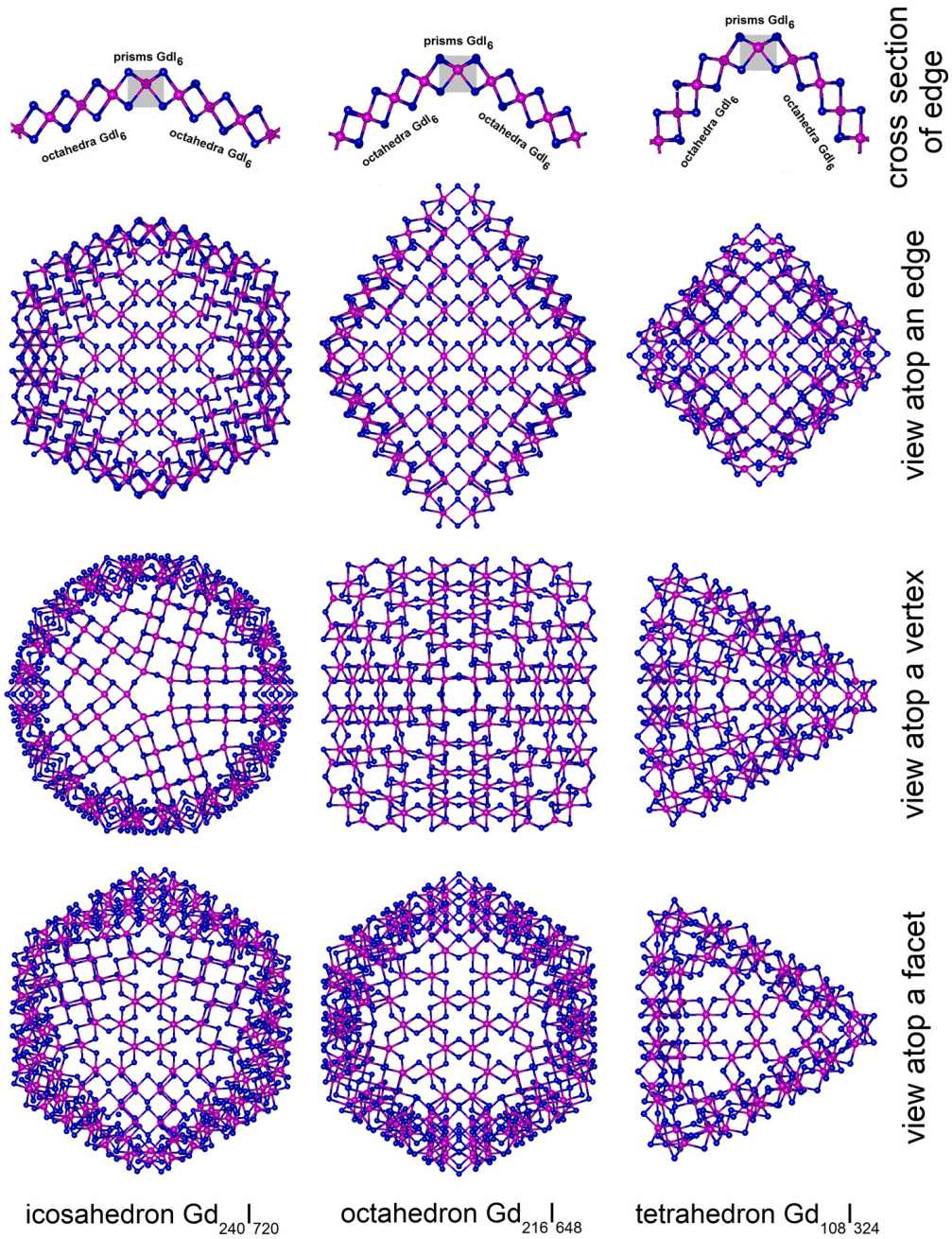

FIG. 1. The ball-and-stick models of GdI_3 fullerenes with optimized structure, revealing the construction principles of their vertices and edges. Gd and I atoms are painted in violet and blue, respectively. DFT calculations

of GdI_3 nanotubes as cylindrical seamless layers revealed their tolerable strain energies ΔE, when comparing to the commercially manufactured MoS_2 or WS_2 nanotubes [14]. Particularly, for nanotubes, the specific ΔE per GdI_3-unit ($\Delta E/N$) obeys classical $\sim 1/R^2$ rule from the elasticity theory for the bending of a layer into cylinder of radius R. The proportionality factor between $\Delta E/N$ and $1/R^2$ for GdI_3 nanotubes is equal to 12.57 (eV·Å^2)/unit, what is found in-between 0.5 (eV·Å^2)/unit for carbon nanotubes and 48.3 (eV·Å^2)/unit for MoS_2 nanotubes. Noteworthy, the strain energy of nanotubes is contributed mostly by elastic deformation of the layer consisting of GdI_6 octahedra. The strain energy of fullerenes should contain also the contribution from GdI_6 prisms as the less favorable coordination polyhedra for GdI_3.

The fully relaxed structures of some GdI_3 fullerenes are shown in the Fig. 1. Morphology and integrity of all these nanoparticles including the smallest representatives are preserved during geometry optimization. No major reconstruction or a crack occurs at vertices or at edges. Facets of all giant representatives become visibly flattened like their parent monolayer.

The specific strain energies $\Delta E/N$ for GdI_3 fullerenes are plotted in Fig. 2(a) against the mean radii $\langle R \rangle$ of their Gd-sublattices. Similarly to carbon fullerenes and nanotubes [30] or sulfide fullerenes and nanotubes [31, 32], $\Delta E/N$ of a GdI_3 fullerene due to the fully closed morphology is one order of magnitude larger, than that for GdI_3 nanotube of the same radius. Like for cylindrical nanotubes, the functions $\Delta E/N$ for all types of fullerenes decrease with the size growth, yet, with the different slopes. An analytical expression for any of these functions can be derived using phenomenological model stipulating a fullerene as nanoparticle with perfect polyhedral morphology. The total energy of a fullerene E can be written as

$$E = N_r \varepsilon_r + N_i \varepsilon_i, \tag{1}$$

where: N_i is the number of Gd atoms forming the flat facets, N_r is the number of Gd atoms forming the edges, and their sum is equal to the total number of stoichiometric GdI_3 units $N = N_i + N_r$. The values ε_i and ε_r are the corresponding specific energies of atoms at facets and edges. N_i and N_r are defined by the number n in accordance to the family: for nanoicosahedra $N_i = 60n(n-1)$, $N_r = 60n$; for nanooctahedra $N_i = 24n(n-1)$, $N_r = 24n$; for nanotetrahedra $N_i = 12n(n-1)$, $N_r = 12n$. Then, specific energy E/N can be written as:

$$\frac{E}{N} = \frac{N_r}{N}\varepsilon_r + \frac{N_i}{N}\varepsilon_i = \frac{1}{n}\varepsilon_r + \frac{n-1}{n}\varepsilon_i, \tag{2}$$

or after transformations

$$\frac{E}{N} = \frac{\sqrt{12}}{\sqrt{N}}(\varepsilon_r - \varepsilon_i) \quad \text{for nanotetrahedra,} \tag{3}$$

$$\frac{E}{N} = \frac{\sqrt{24}}{\sqrt{N}}(\varepsilon_r - \varepsilon_i) \quad \text{for nanooctahedra,} \tag{4}$$

$$\frac{E}{N} = \frac{\sqrt{60}}{\sqrt{N}}(\varepsilon_r - \varepsilon_i) \quad \text{for nanoicosahedra.} \tag{5}$$

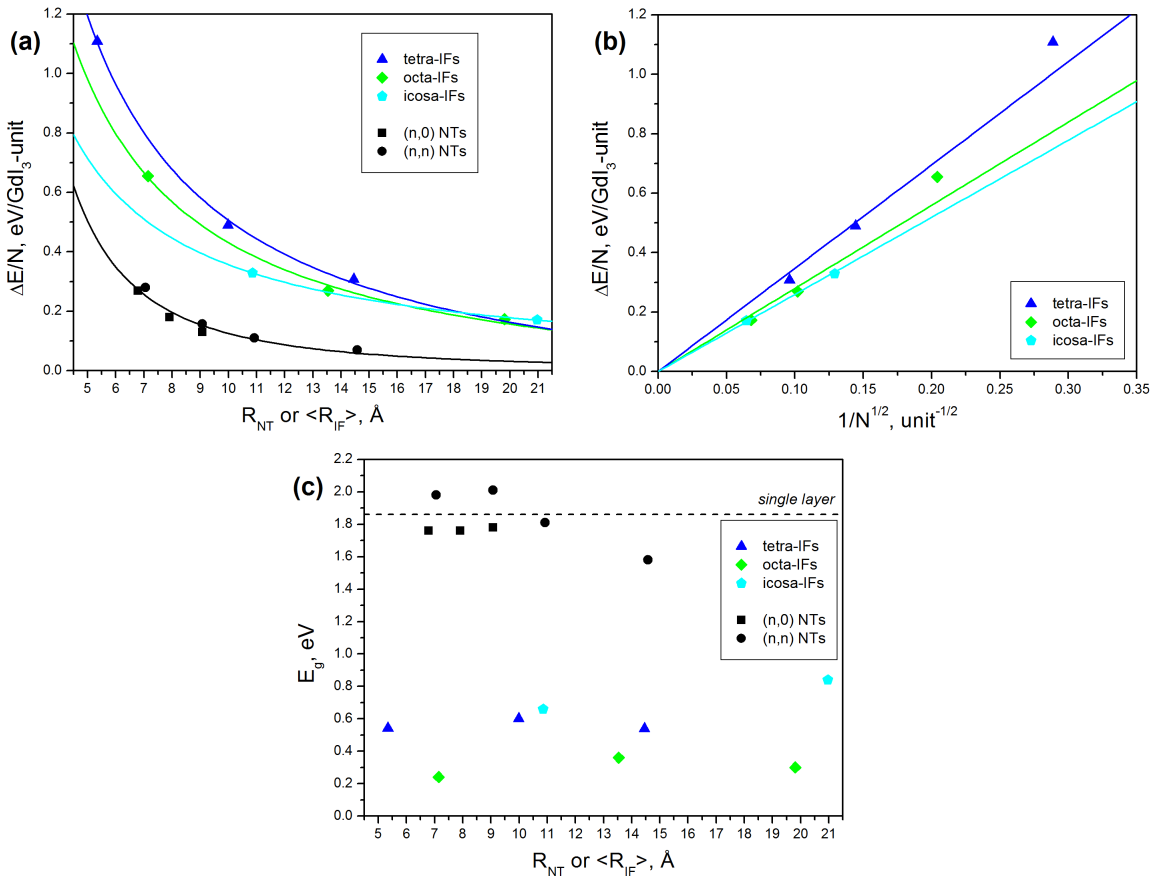

FIG. 2. Thermodynamic and electronic properties for GdI_3 fullerenes (IFs) of different morphology in comparison to those for parent monolayer and for GdI_3 nanotubes (NTs) of different chirality [14]: (a) specific strain energies $\Delta E/N$ for various nanostructures depending on the mean particles' radii R and their morphology; (b) specific strain energies $\Delta E/N$ for fullerenes depending on the number N of constituting units; (c) band gap values E_g. DFT calculations

The value $(\varepsilon_r - \varepsilon_i)$ is nothing more, than the specific strain energy contributed exclusively by an edge atom, i.e. excessive energy of GdI_6 prism relative to GdI_6 octahedron. Therefore, Eqs. (3–5) may be ascribed to homogeneous linear functions:

$$\frac{\Delta E}{N} = \frac{\sqrt{12}}{\sqrt{N}}\Delta\varepsilon_r \quad \text{for nanotetrahedra,} \tag{6}$$

$$\frac{\Delta E}{N} = \frac{\sqrt{24}}{\sqrt{N}}\Delta\varepsilon_r \quad \text{for nanooctahedra,} \tag{7}$$

$$\frac{\Delta E}{N} = \frac{\sqrt{60}}{\sqrt{N}}\Delta\varepsilon_r \quad \text{for nanoicosahedra.} \tag{8}$$

These strain energies for GdI_3 fullerenes show a somewhat different behavior, than that for carbon fullerenes. They appear to be proportional to $1/\sqrt{N}$, whereas for carbon fullerenes $\Delta E/N$ is proportional to $1/N$ [30]. It points to the dominant role of strain at edges in regulation of thermodynamic stability of a whole GdI_3 fullerene. The data on the total energies of GdI_3 fullerenes available from DFT calculations were fitted using Eqs. (6–8), estimating $\Delta\varepsilon_r = 1.00$ eV/unit$^{1/2}$, $\Delta\varepsilon_r = 0.57$ eV/unit$^{1/2}$ and $\Delta\varepsilon_r = 0.34$ eV/unit$^{1/2}$ for tetrahedral, octahedral and icosahedral morphology, respectively (Fig. 2 (b)). Such order of $\Delta\varepsilon_r$ correlates with the local curvature at edges within particular morphology: from the largest curvature within tetrahedron to the least one within icosahedron. Obviously, GdI_3 fullerenes would tend to form icosahedral and octahedral morphologies, if synthesized.

3.3. Electronic structure of GdI_3 fullerenes

The calculated densities of electronic states (DOS) for several fullerenes and monolayer of GdI_3 are visualized in Fig. 3. Irrespective of size and morphology, electronic structure of different GdI_3 fullerenes is qualitatively similar and mainly resembles that for monolayer or nanotubes of GdI_3 [14]. In accordance to the polar covalent character of the Gd–I bonding, the topmost valence band consists of mainly I5p-states with a small admixture of Gd6s- and Gd5d-states and settles at $-1... - 4$ eV below Fermi level. While this valence band is characterized by a minor spin polarization, the conduction band at $+1... + 2.5$ eV above Fermi level is spin-polarized and consists of Gd5d-states grouped in two subbands in accordance to the splitting of d-orbitals in octahedral crystal field. The bands' splitting becomes smoothed in the case of fullerenes, since their symmetries possess a greater variety of inequivalent atom types, than symmetries of monolayer or nanotubes do. Occupied and unoccupied Gd4f-states form two strongly localized narrow bands of different spin-polarization at energies around -7.5 eV and $+3.5$ eV, respectively.

Therefore, all studied GdI_3 fullerenes should be magnetic semiconductors like their parent monolayer. Monolayer possesses the fundamental band gap E_g of at least 1.8 eV with the gap edges formed by states of the same spin projection and with indirect $\Gamma - M$ transition. The calculated E_g is found underestimated, when comparing to the experimental value E_g of 5.1 eV [33]. Such a mismatch is typical for standard calculational DFT schemes [34] and does not preclude discussion of relative values. When comparing with monolayer and nanotubes, the values E_g for fullerenes can be found distinctly smaller as 0.2 –0.8 eV (Fig. 2(c)). This reduction of the band gap has two origins: first, the presence of prismatic coordination polyhedra with another crystal field for splitting of Gd5d-orbitals and, second, an enhanced overlap between Gd5d- and I5p-orbitals from atoms at internal surface of the mechanically stressed parts of fullerene – vertices and edges. Electronic levels of these orbitals tend to localize at the bottom of conduction band and at the top of valence band and, in some cases, they even separate as localized mid-gap states (Fig. 3).

A little is known about magnetic transition in the lattice of GdI_3. The chemically related bulk trichloride $GdCl_3$ orders ferromagnetically below 2.2 K, the bulk $GdBr_3$ becomes magnetic below 1.3 K with the not yet clearly defined type of ordering, while the bulk GdI_3 might be magnetic below 1 K [35]. DFT+U calculations claimed that, GdI_3 monolayer is antiferromagnetic as bipartite lattice, yet, neither the used U parameter nor independence of energy difference between magnetic orderings on U was verified [36].

The presented here DFT calculations vote for ferromagnetic lattice of GdI_3 monolayer with energy gain 5.7 meV/unit over its antiferromagnetic bipartite lattice. The model of octahedral fullerene $(GdI_3)_{96}$ offers an opportunity to study magnetic ordering of GdI_3 monolayer at zero-dimensionality. First, it contains only even cycles of Gd-sublattice, hence, it is magnetically unfrustrated and might appear as bipartite lattice. Second, two types of coordination polyhedra (prisms GdI_6 and octahedra GdI_6 forming the edges and the facets) are given in equimolar ratio, hence, suggesting a configuration with the antiferromagnetically ordered edges and facets. The results approve a preservation of ferromagnetic ordering within single GdI_3 layer even folded into fullerene with the energy gains 2.7 and 0.5 meV/unit over the first and the second configurations, respectively.

4. Summary

In summary, the models of GdI_3 fullerenes were constructed and fullerenes' stability and electronic structure were studied by means of quantum-chemical calculations. The results reveal a higher stability of GdI_3 fullerenes with octahedral and icosahedral shapes, than these with tetrahedral shape. The derived functional dependence of stability on the size

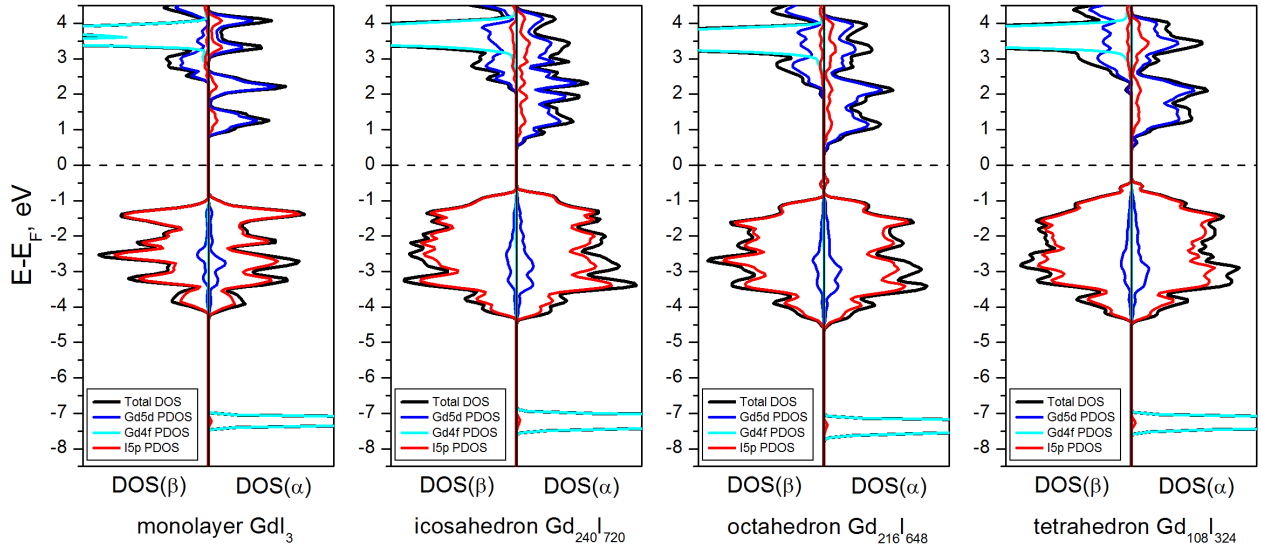

FIG. 3. Total and partial densities of spin-projected electronic states (DOS) for monolayer of GdI_3 and descendant fullerenes of different morphology. DFT calculations

confirms that, the strain at the fullerenes' edges contributes the most into the total strain energy of fullerenes. The electronic structure of all GdI_3 fullerenes considered here has a HOMO-LUMO gap of 0.2 – 0.8 eV, which is narrower than the band gap of GdI_3 monolayer due to an enhanced overlap between Gd5d- and I5p-orbitals at internal curved surface of the vertices and edges.

The present calculations do not hint on fabrication route to GdI_3 fullerenes. Though, by analogy to known fullerenes of layered dihalogenides [15–18], the physical methods employing high energetic processes like laser ablation from or electron-beam irradiation of the bulk material show a great promise.

References

[1] Luo X.-M., Hu Z.-B., Lin Q.-F., Cheng W., Cao J.-P., Cui C.-H., Mei H., Song Y., Xu Y. Exploring the Performance Improvement of Magnetocaloric Effect Based Gd-Exclusive Cluster Gd_{60}. *J. of the American Chemical Society*, 2018, **140**, P. 11219–11222.

[2] Xu Q., Liu B., Ye M., Zhuang G., Long L., Zheng L. Gd(OH)F_2: A Promising Cryogenic Magnetic Refrigerant. *J. of the American Chemical Society*, 2022, **144**, P. 13787–13793.

[3] Iyad N., Ahmad M.S., Alkhatib S.G., Hjouj M. Gadolinium contrast agents – challenges and opportunities of a multidisciplinary approach: Literature review. *European J. of Radiology Open*, 2023, **11**, 100503.

[4] Thomsen H.S., Almén T., Morcos S.K., members of the Contrast Media Safety Committee of ESUR. Gadolinium-containing contrast media for radiographic examinations: a position paper. *European Radiology*, 2002, **12**, P. 2600–2605.

[5] Saha S., Ntarisa A.V., Quang N.D., Kim H.J., Kothan S., Kaewkhao J. Synthesis and elemental analysis of gadolinium halides (GdX_3) in glass matrix for radiation detection applications. *Optical Materials*, 2022, **129**, 112490.

[6] Caravan P., Ellison J.J., McMurry T.J., Lauffer R.B. Gadolinium(III) Chelates as MRI Contrast Agents: Structure, Dynamics, and Applications. *Chemical Reviews*, 1999, **99**, P. 2293–2352.

[7] Ghiassi K.B., Olmstead M.M., Balch A.L. Gadolinium-containing endohedral fullerenes: structures and function as magnetic resonance imaging (MRI) agents. *Dalton Transactions*, 2014, **43**, P. 7346–7358.

[8] Sitharaman B., Kissell K.R., Hartman K.B., Tran L.A., Baikalov A., Rusakova I., Sun Y., Khant H.A., Ludtke S.J., Chiu W., Laus S., Tóth É., Helm L., Merbach A.E., Wilson L.J. Superparamagnetic gadonanotubes are high-performance MRI contrast agents. *Chemical Communications*, 2005, **2005**, P. 3915–3917.

[9] Sitharaman B., van der Zande M., Ananta J.S., Shi X., Veltien A., Walboomers X.F., Wilson L.J., Mikos A.G., Heerschap A., Jansen J.A. Magnetic resonance imaging studies on gadonanotube-reinforced biodegradable polymer nanocomposites. *J. of Biomedical Materials Research A*, 2010, **93**, P. 1454–1462.

[10] Hartman K.B., Laus S., Bolskar R.D., Muthupillai R., Helm L., Toth E., Merbach A.E., Wilson L.J. Gadonanotubes as Ultrasensitive pH-Smart Probes for Magnetic Resonance Imaging. *Nano Letters*, 2008, **8**, P. 415–419.

[11] Fidiani E., Costa P.M.F.J., Wolter A.U.B., Maier D., Buechner B., Hampel S. Magnetically Active and Coated Gadolinium-Filled Carbon Nanotubes. *The J. of Physical Chemistry C*, 2013, **117**, P. 16725–16733.

[12] Anumol E.A., Enyashin A.N., Batra N.M., Costa P.M.F.J., Deepak F.L. Structural and chemical analysis of gadolinium halides within WS_2 nanotubes. *Nanoscale*, 2016, **8**, 12170.

[13] Deepak F.L., Enyashin A.N. Capillary Imbibition of Gadolinium Halides into WS_2 Nanotubes: a Molecular Dynamics View. *Israel J. of Chemistry*, 2017, **57**, P. 501–508.

[14] Batra N., Anumol E.A., Smajic J., Enyashin A.N., Deepak F.L., Costa P.M.F.J. Morphological Phase Diagram of a Metal Halide Encapsulated in Carbon Nanotubes. *The J. of Physical Chemistry C*, 2018, **122**, P. 24967–24976.

[15] Hacohen Y.R., Popovitz-Biro R., Grunbaum E., Prior Y., Tenne R. Vapor–Liquid–Solid (VLS) Growth of $NiCl_2$ Nanotubes via Reactive Gas Laser Ablation. *Advanced Materials*, 2002, **14**, P. 1075–1078.

[16] Bar-Sadan M., Popovitz-Biro R., Prior Y., Tenne R. Closed-cage (fullerene-like) structures of $NiBr_2$. *Materials Research Bulletin*, 2006, **41**, P. 2137–2146.

[17] Tenne R., Popovitz-Biro R., Twersky A., Hacohen Y.R. Nanoparticles of $CdCl_2$ with closed cage structures. *Israel J. of Chemistry*, 2001, **41**, P. 7–14.

[18] Sallacan N., Popovitz-Biro R., Tenne R. Nanoparticles of CdI_2 with closed cage structures obtained via electron-beam irradiation. *Solid State Sciences*, 2003, **5**, P. 905–908.

[19] Wang X., Li Y. Fullerene-Like Rare-Earth Nanoparticles. *Angewandte Chemie International Edition*, 2003, **42**, P. 3497–3500.

[20] Bar-Sadan M., Kaplan-Ashiri I., Tenne R. Inorganic fullerenes and nanotubes: Wealth of materials and morphologies. *European Physical J. Special Topics*, 2007, **149**, P. 71–101.

[21] Enyashin A.N. Theoretical studies of inorganic fullerenes and fullerene-like nanoparticles. *Israel J. of Chemistry*, 2010, **50**, P. 468–483.

[22] Ordejón P., Artacho E., Soler J.M. Self-consistent order-N density-functional calculations for very large systems. *Physical Review B*, 1996, **53**, R10441.

[23] García A., Papior N., Akhtar A., Artacho E., Blum V., Bosoni E., Brandimarte P., Brandbyge M., Cerdá J.I., Corsetti F., Cuadrado R., Dikan V., Ferrer J., Gale J., García-Fernández P., García-Suárez V.M., García S., Huhs G., Illera S., Korytár R., Koval P., Lebedeva I., Lin L., López-Tarifa P., Mayo S.G., Mohr S., Ordejón P., Postnikov A., Pouillon Y., Pruneda M., Robles R., Sánchez-Portal D., Soler J.M., Ullah R., Yu V.W., Junquera J. SIESTA: Recent developments and applications. *The J. of Chemical Physics*, 2020, **152**, 204108.

[24] Asprey L.B., Keenan T.K., Kruse F.H. Preparation and Crystal Data for Lanthanide and Actinide Triiodides. *Inorganic Chemistry*, 1964, **3**, P. 1137–1141.

[25] Beck H.P., Gladrow E. Zur Hochdruckpolymorphie der Seltenerd-Trihalogenide. *Zeitschrift für Anorganische und Allgemeine Chemie*, 1979, **453**, P. 79–92.

[26] Hargittai I. In the shadow's shadow: Ivan V. Stankevich and C_{60}. *Structural Chemistry*, 2025, **36**, P. 1531–1533.

[27] Huisman R., de Jonge R., Haas C., Jellinek F. Trigonal-prismatic coordination in solid compounds of transition metals. *J. of Solid State Chemistry*, 1971, **3**, P. 56–66.

[28] Miura A., Tadanaga K., Magome E., Moriyoshi C., Kuroiwa Y., Takahiro T., Kumada N. Octahedral and trigonal-prismatic coordination preferences in Nb-, Mo-, Ta-, and W-based ABX_2 layered oxides, oxynitrides, and nitrides. *J. of Solid State Chemistry*, 2015, **229**, P. 272–277.

[29] Kasten A., Müller P.H., Schienle M. Magnetic ordering in GdI_2. *Solid State Communications*, 1984, **51**, P. 919–921.

[30] Seifert G., Vietze K., Schmidt R. Ionization energies of fullerenes – size and charge dependence. *J. of Physics B*, 1996, **29**, P. 5183–5192.

[31] Bar-Sadan M., Enyashin A.N., Gemming S., Popovitz-Biro R., Hong S.Y., Prior Y., Tenne R., Seifert G. Structure and Stability of Molybdenum Sulfide Fullerenes. *The J. of Physical Chemistry B*, 2006, **110**, P. 25399–25410.

[32] Enyashin A.N., Brontvein O., Seifert G., Tenne R. Structure and Stability of GaS Fullerenes and Nanotubes. *Israel J. of Chemistry*, 2017, **57**, P. 529–539.

[33] Birowosuto M.D., Dorenbos P. Novel γ- and X-ray scintillator research: on the emission wavelength, light yield and time response of Ce^{3+} doped halide scintillators. *Physica Status Solidi A*, 2009, **206**, P. 9–20.

[34] Li W., Walther C.F.J., Kuc A., Heine T. Density Functional Theory and Beyond for Band-Gap Screening: Performance for Transition-Metal Oxides and Dichalcogenides. *J. of Chemical Theory and Computation*, 2013, **9**, P. 2950–2958.

[35] Hovi V., Vuola R., Salmenperä L. The Specific Heats of $GdCl_3$, $GdBr_3$, and GdI_3 at Low Temperatures. *J. of Low Temperature Physics*, 1970, **2**, P. 383–387.

[36] You H., Zhang Y., Chen J., Ding N., An M., Miao L., Dong S. Peierls transition driven ferroelasticity in the two-dimensional d-f hybrid magnets. *Physical Review B*, 1970, **2**, P. 383–387.

Submitted 27 June 2025; accepted 18 August 2025

Information about the authors:

Andrey N. Enyashin – Institute of Solid State Chemistry UB RAS, Ekaterinburg, Russia; ORCID 0000-0001-6195-7971); enyashin@ihim.uran.ru